photonics

MDPI

Article

The Origin of Threshold Reduction in Random Lasers Based on MoS_2/Au NPs: Charge Transfer

Yanyan Huo [1,2], Ke Sun [1,2], Yuqian Zhang [1,2], Weihao Liu [1,2], Junkun Wang [1,2], Yuan Wan [1,2], Lina Zhao [1,2], Tingyin Ning [1,2], Zhen Li [1,2,*] and Yingying Ren [1,2,*]

[1] Shandong Provincial Key Laboratory of Optics and Photonic Device & Shandong Provincial Engineering and Technical Center of Light Manipulations, School of Physics and Electronics, Shandong Normal University, Jinan 250358, China; yanyanhuo2014@sdnu.edu.cn (Y.H.); 2021020560@stu.sdnu.edu.cn (K.S.); 2022020565@stu.sdnu.edu.cn (Y.Z.); 2021020567@stu.sdnu.edu.cn (W.L.); 2021020605@stu.sdnu.edu.cn (J.W.); wanyuan@sdnu.edu.cn (Y.W.); lnzhao@sdnu.edu.cn (L.Z.); ningtingyin@sdnu.edu.cn (T.N.)

[2] Collaborative Innovation Center of Light Manipulations and Applications, Shandong Normal University, Jinan 250358, China

* Correspondence: 619052@sdnu.edu.cn (Z.L.); ryywly@sdnu.edu.cn (Y.R.)

Abstract: Random lasers have attracted much attention in recent years owing to their advantages of a simple fabrication process, low processing cost, and material flexibility for any lasing wavelengths. They provide a roadmap for the design of ultra-bright lighting, displays, etc. However, the threshold reduction in random nanolasers remains a challenge in practical applications. In this work, lower-threshold random laser action from monolayer molybdenum disulfide film-encapsulated Au nanoparticles (MoS_2/Au NPs) is demonstrated. The observed laser action of the MoS_2/Au NPs shows a lower threshold of about 0.564 μJ/mm^2, which is about 46.2% lower than the threshold of random lasers based on Au NPs. We proposed that the charge transfer between MoS_2 and the gain material is the main reason for the reduction in the random laser threshold. The finite-difference time-domain (FDTD) method was used to calculate the lasing action of these two nanostructures. When charge transfer is taken into account, the theoretically calculated threshold of the MoS_2/Au NPs is reduced by 46.8% compared to Au NP samples, which is consistent with the experimental results. This study provides a new mechanism to achieve low-threshold and high-quality random lasers, which has the potential to facilitate the application of random lasers and the development of high-performance optoelectronic devices.

Keywords: random laser; low threshold; charge transfer; MoS_2; Au NPs

check for updates

Citation: Huo, Y.; Sun, K.; Zhang, Y.; Liu, W.; Wang, J.; Wan, Y.; Zhao, L.; Ning, T.; Li, Z.; Ren, Y. The Origin of Threshold Reduction in Random Lasers Based on MoS_2/Au NPs: Charge Transfer. *Photonics* **2024**, *11*, 168. https://doi.org/10.3390/photonics11020168

Received: 12 January 2024
Revised: 4 February 2024
Accepted: 6 February 2024
Published: 9 February 2024

Copyright: © 2024 by the authors. Licensee MDPI, Basel, Switzerland. This article is an open access article distributed under the terms and conditions of the Creative Commons Attribution (CC BY) license (https://creativecommons.org/licenses/by/4.0/).

1. Introduction

Random lasers have attracted great attention due to their unique physical mechanisms and applications in fields such as biosensing, optical information processing, and so on. They have the advantages of simple manufacturing processes [1], low processing costs [2], and low flexibility for materials of any laser wavelength [3]. In contrast to traditional lasers, the feedback amplification in a random laser is not provided by a cavity formed by reflecting elements but by the disorder-induced scattering of light in the random medium [4,5]. As the research on random lasers has improved, significant progress has been made in reducing their thresholds [6–9], regulating them [10], and finding new materials [11]. Reducing the random laser threshold can increase the efficiency and lifespan of a laser, as well as reduce energy consumption and costs, which will promote the miniaturization and integration of random lasers. However, threshold reduction remains a challenge in practical applications [12,13].

The enhanced localization of electromagnetic fields and scattering effects can reduce the threshold of random lasers. Zhao et al. demonstrated that the threshold of a random laser is reduced from ~2.0 mJ/cm^2 to ~1.6 mJ/cm^2 when a layer of polymethyl methacrylate

(PMMA)-doped CdSe/ZnS colloidal quantum dots (CQDs) is coated onto Ag nano-island structures, which is caused by the strong surface plasmon resonance and plasmonic scattering of the Ag nano-islands [14]. Wan et al. found that a random laser containing TiN nanoparticles (NPs) had a lower threshold than a random laser containing TiO_2 NPs due to the stronger localized surface plasmon resonance of TiN NPs [15]. There are also some works that have effectively reduced the threshold of random lasers by designing structures that support strong surface plasmons [16,17]. Moreover, increasing the scattering cross-section can increase the probability of photon scattering in random media, which can lower the threshold of random lasers. Some works have proposed that adding two-dimensional materials to random laser structures can effectively lower the threshold. Wan et al. demonstrated that the lasing threshold of a random laser with graphene nanosheets is only about 31.8% of that of a random laser without graphene nanosheets [18]. Shen et al. confirmed that the introduction of graphene can reduce the threshold of a random laser by 34.8% [19]. Roy et al. also reduced the threshold of a random laser by utilizing vertically oriented graphene nanowalls [20].

Two-dimensional materials are a current research hotspot [21,22], among which molybdenum disulfide (MoS_2) is a promising candidate for two-dimensional (2D) transition-metal dichalcogenides. Monolayer MoS_2 has a direct bandgap of 1.9 eV, which makes it a very promising optoelectronic material for potential applications in solar cells [23,24], photodetectors [25], optoelectronic converters, and so on [26]. MoS_2 is also used in the field of surface-enhanced Raman spectroscopy (SERS) because it can undergo a charge transfer with dye molecules, resulting in a chemical enhancement that increases the SERS signal intensity and sensitivity, which has been demonstrated experimentally and theoretically [27–29]. With deep research into the unique structure and properties of MoS_2, nanolasers based on MoS_2 have been studied. However, it is primarily used to modulate nanolasers' characteristics and as a gain material to realize nanolasers [30]. To the best of our knowledge, there are almost no studies reporting that the charge transfer between MoS_2 and dye molecules can reduce the threshold of nanolasers. However, charge transfer has been proposed as a possible reason for random lasing [31].

Herein, we demonstrate that the charge transfer between MoS_2 and the gain material can reduce the threshold of a random laser. We fabricated high-quality, large-area, and uniform Au NPs, and then MoS_2 was directly fabricated onto the Au NPs to form MoS_2-encapsulated Au NPs (MoS_2/Au NPs). A rhodamine 6G (R6G)-doped PMMA layer was spun onto the Au NPs and MoS_2/Au NPs to form random laser structures based on the waveguide effect. We studied the random laser's properties based on Au NPs and MoS_2/Au NPs and found that after the Au NPs were encapsulated in MoS_2, the threshold of the random laser could be reduced by 46.2%. Then, the lasing threshold was calculated by using commercial simulation software (FDTD Solutions) based on the finite difference in the time domain method, and we found that the charge transfer between MoS_2 and R6G is the main reason for the reduction in the random laser threshold. This paper explores a new mechanism to achieve low-threshold random lasers and the potential of using 2D materials to improve their performance.

2. Preparation of Experimental Sample

A schematic diagram showing the preparation process of the Au NPs and MoS_2/Au NP samples is shown in Figure 1. It mainly consists of the following steps: 1. A thermal-evaporation system (1 Å/s rate, 10^{-3} Pa) was used to deposit about a 12 nm Au film on the SiO_2 plates. 2. The SiO_2 plates with gold films were placed in a quartz tube at a pressure of 10^{-3} Pa, and then the quartz tube was heated to 600 °C with a flow of Ar/H_2 of about 100/20 sccm for the annealing treatment. After this process, the gold film transformed into randomly distributed Au NPs. 3. A mixture of ethylene glycol (1 mL) and high-purity $(NH_4)_2MoS_4$ (0.01 g) was ultrasonically treated for 20 min until they entirely dissolved, then the $(NH_4)_2MoS_4$ solution was spin-coated onto the Au NP samples using a spinner with a rotation speed of 2000 rpm for 3 min. 4. In order to remove sulfide in the precursor

solution and obtain MoS_2, we continued annealing the samples at 500 °C with the gas flow (Ar/H_2 about 80/20 sccm). After the samples cooled to an ambient temperature, a MoS_2 film formed on the surface of the Au NPs. 5. The samples were then treated with Ar plasma (13.56 MHz RF source) with power of 10 W and a pressure of 10 Pa, which thins down the MoS_2 film on the Au NPs to a monolayer. 6. The random laser studied here is based on the waveguide effect. We mixed 40 mg/mL polyvinyl alcohol aqueous (PVA) solution and 3 mg/mL R6G aqueous solution in a 1:1 volume ratio. Then, the mixed solution was ultrasonically treated for 20 min until they were completely mixed. The mixed solution was spun onto the surface of Au NPs and MoS_2/Au NPs samples to obtain the random laser samples. R6G serves as the gain material, Au NPs or MoS_2/Au NPs serve as multiple scattering, and PVA forms the waveguide layer. When the pump laser is irradiated on the structure, light is strongly scattered by the Au NPs or MoS_2/Au NPs. A large part of the scattered light was reflected totally back at the PVA/air interface to propagate within the active waveguide and scattered further by the Au NPs or MoS_2/Au NPs, which experiences strong amplification through stimulated emission, through which a random lasing can be generated [32].

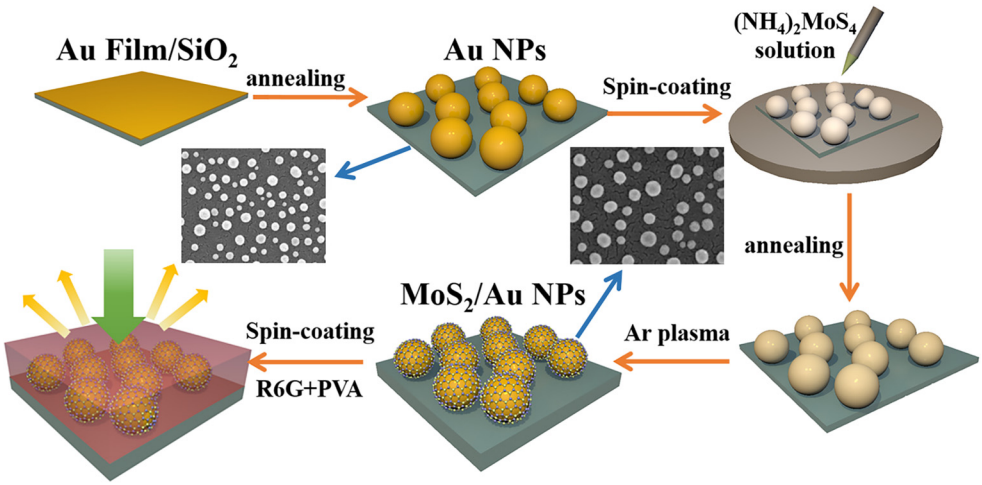

Figure 1. Schematic illustration of the process of random laser based on MoS_2/Au NPs.

3. Results and Discussion

The Au NPs were obtained by annealing the gold film, which is more uniform, as shown by the SEM in Figure 2a. The uniform and large-area MoS_2 films were synthesized by thermal decomposition. By growing directly on the surface of Au NPs, MoS_2 can be very tightly attached to the surface of the gold nanoparticles, which is shown in Figure 2b; the samples thus formed are more favorable for random laser generation than the $MoS_2-Au-MoS_2$ structure [33]. The MoS_2/Au NPs formed by this method not only effectively suppress lattice defects but also reduce the scattering enhancement caused by the introduction of MoS_2. After the MoS_2/Au NPs were dissolved in an ethanol solution, we captured the TEM images of the MoS_2/Au NPs, as shown in Figure 2c,d, where the MoS_2 is tightly wrapped around the surface of Au NPs. The thickness of the MoS_2 layer is about 0.65 nm, indicating that the MoS_2 is monolayer. In addition, a Raman spectrometer (Horiba HR Evolution 800) with laser excitation (2.4 mW laser power, 532 nm excitation, acquisition time of 4 s, etc.) was used to carry out the Raman analysis of the MoS_2/Au NPs. As shown in Figure 2e, there are two peaks at 384.2 and 403.9 cm^{-1}, which correspond to the in-plane $E_1{}^{2g}$ and out-of-plane A_{1g} modes of $2H-MoS_2$, respectively. These characteristic peaks once again indicate that the gold particles are coated with MoS_2.

The SEM images in Figure 2a,b show the morphological characteristics of Au NPs and MoS_2/Au NPs. These nanoparticles are distributed relatively uniformly, with an average size of about 80 nm. We measured the absorption spectra of the Au NPs and MoS_2/Au NPs using $UV-vis$ spectroscopy ($UV-vis$), as shown in Figure 2f. Their absorption peaks

are at 539.2 and 570.5 nm, respectively. The absorption of MoS_2/Au NPs undergoes a red shift compared with Au NPs. This is mainly attributed to the close relationship between the surface plasmon resonance absorption peaks of Au NPs and the ambient medium of the Au NPs and an increase in the refractive index of the dielectric ambient when the Au NPs are covered with MoS_2, resulting in the red-shifted surface plasmon resonance absorption peaks. The photoluminescence (PL) peak of R6G is at 575 nm, as shown by the blue line in Figure 2f. It can be seen that both the absorption spectra of Au NPs and MoS_2/Au NPs can overlap with the PL spectrum of R6G, which makes it easier to achieve random lasing. The absorption peak of the MoS_2/Au NPs is closer to the fluorescence peak of R6G, which will facilitate their interactions with the gain material [32]. In addition, the type and size of metal nanoparticles also affect the PL [34], potentially leading to an increase in the laser threshold if the luminescence peak of R6G does not overlap well with the absorption of the sample.

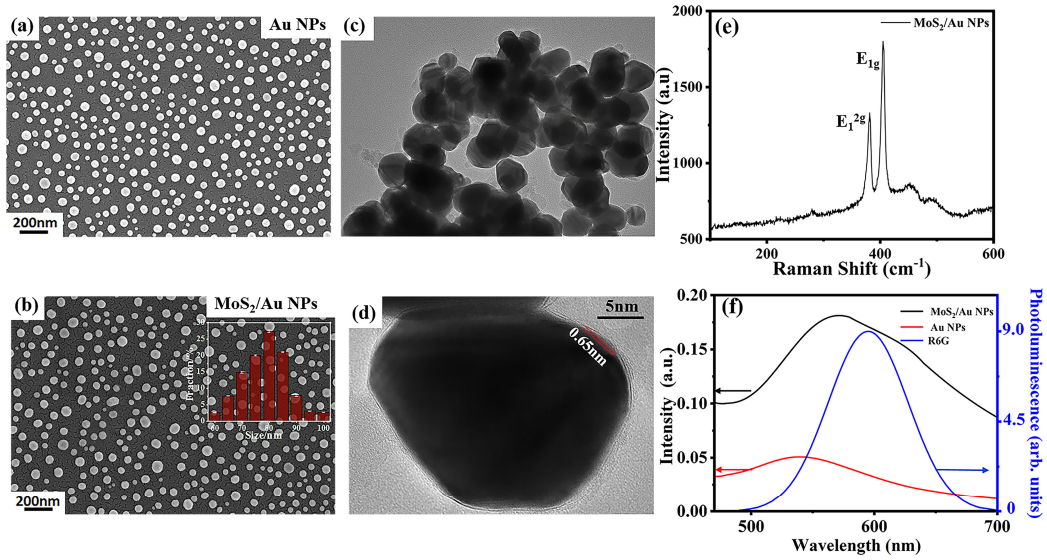

Figure 2. SEM image of Au NPs (**a**) and MoS_2/Au NPs (**b**) (inset is a particle size distribution statistical chart of MoS_2/Au NPs); (**c**,**d**) TEM images of MoS_2/Au NPs with different resolutions; (**e**) Raman spectra of MoS_2/Au NPs; (**f**) the UV−vis absorption spectra of Au NPs (red), MoS_2/Au NPs (black), and PL spectrum of R6G (blue).

We measured the random lasing action of the random laser based on Au NPs and MoS_2/Au NPs. The schematic diagram of the experimental setup is shown in Figure 3a. In the experiment, an Nd:YAG mode-locked laser (532 nm, 25 ps, 10 Hz) was used as a pump source. The energy of the pump light is manipulated by adjusting the energy attenuator. The pump light is divided into two beams by the beam splitter. One beam is used to record the energy of the pump light, and the other one is used to excite the samples. The light emitted from the samples is collected by an optical fiber spectrometer for analysis. Figure 3b shows the emission spectra of the Au NPs sample as a function of the energy. The wavelength, shown by the dashed line, is the pump light. When the pump energy is small, the emission spectrum is very wide, which is the spontaneous emission spectrum of the R6G. As the pump light energy continues to increase, a narrow peak appears at 575 nm, which is the random laser peak. Figure 3c shows the variation in the emission peak intensity and FWHM of the emission spectrum with the pump energy. It can be seen that when the pump energy exceeds 1.048 μJ/mm^2, the peak intensity increases rapidly, and the FWHM of the spectrum drops sharply, from about 66 nm to 15 nm. This is a typical stimulated emission behavior in a laser system. This pump energy is called the lasing threshold of the random laser based on Au NPs. The emission spectra of the MoS_2/Au NPs samples with different pump energies are shown in Figure 3d. The variation trend of the spectra with respect to pump energy is essentially the same as that of the Au NPs. The lasing

action can still occur as the pump energy increases. However, the lasing red peak shifts to 591 nm due to the addition of MoS_2. Figure 3e shows the peak intensity and FWHM of the emission spectrum of MoS_2/Au NPs as a function of the pump energy. The lasing threshold for the random laser based on MoS_2/Au NPs is approximately 0.564 μJ/mm^2, which is approximately 46.2% lower than the threshold of the random laser based on Au NPs. We also measured the ablation threshold of the sample as 135 μJ/mm^2; the sample was not optically damaged during the experiment. In addition, we found that for the MoS_2/Au NPs random laser, the intensity of the emission peak was stronger, and the width of the lasing peak was wider than that of the Au NPs. These phenomena are all attributed to the charge transfer between MoS_2 and R6G, which we will discuss in detail below. It should be noted that the pump laser spectra overlap with the spontaneous emission spectra of R6G. We carried out peak fitting when measuring the FWHM.

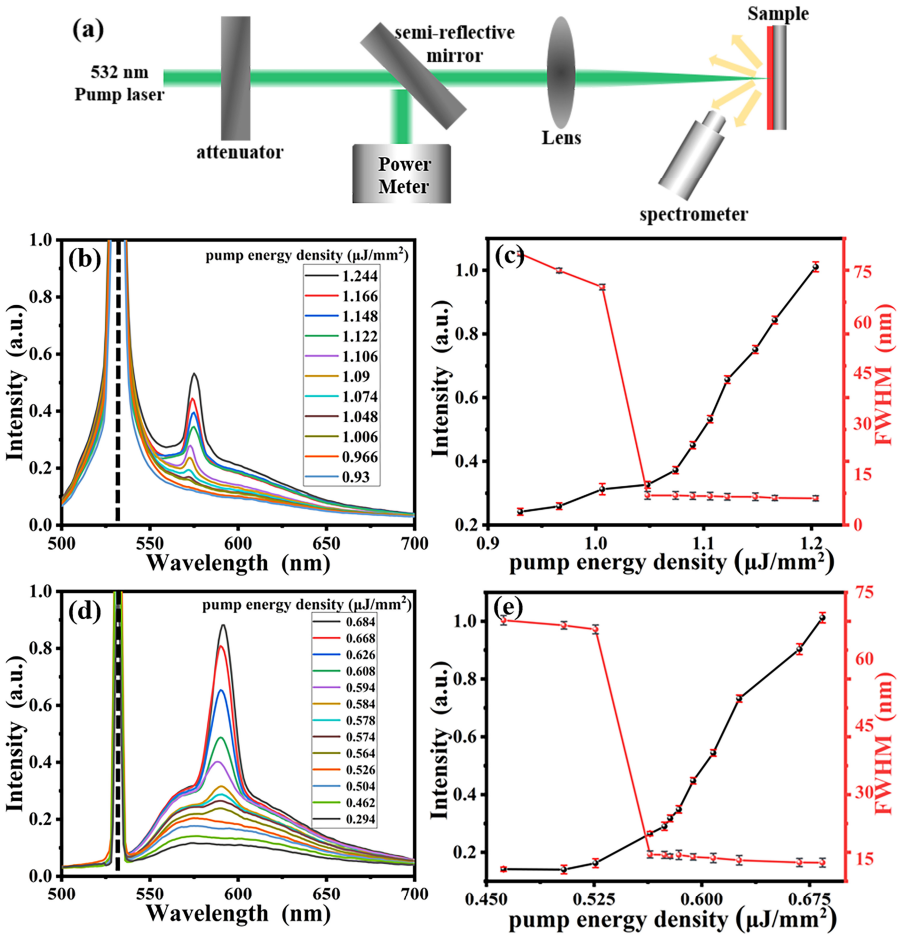

Figure 3. (**a**) Schematic diagram of the experimental setup; (**b**,**d**) the emission spectra of the Au NPs (**b**) and MoS_2/Au NPs (**d**) lasing samples at different pump energies; and (**c**,**e**) the lasing peak intensity and FWHM of the corresponding emission peak as a function of the pump energy.

We calculated the properties and laser actions of the Au NPs and MoS_2/Au NPs using FDTD Solutions software. In order to save computational memory and time, we calculated the scenario in which four nanoparticles are arranged along the polarization direction of the incident light. The structure mainly consists of a gain material layer, a substrate, the Au NPs, and a MoS_2 layer. The gain material layer is composed of PVA doped with R6G (n_{PVA} = 1.52), the substrate material is silica with n_s = 1.48, and the refractive index of Au is taken from experimental data [35]. The radius of the Au NPs was set to 40 nm, and the gap between them was 5 nm. The Au NPs were coated with a monolayer MoS_2, which had a thickness of 0.65 nm. When the 532 nm pump light was incident, the dielectric

constant of MoS_2 was set as $\varepsilon = 5.9 + i1.4$. The gain material used a four-level, two-electron model to describe the outcome. The four energy levels involved in laser generation include ground-state level E_0, lower laser level E_1, upper laser level E_2 (metastable level), and excited-state level E_3. The pumped light excites electrons from the ground-state (E_0) level to the excited-state (E_3) level and then relaxes it to the E_2 level, and the transition between E_2 and E_1 is responsible for the coherent emission of laser light. N_0, N_1, N_2, and N_3 represent the population distribution of electrons in the respective energy levels, which satisfy the following equation [36,37]:

$$\begin{aligned}
\frac{dN_3}{dt} &= \frac{N_3(1-N_2)}{\tau_{32}} - \frac{N_3(1-N_0)}{\tau_{30}} + \frac{1}{\hbar\omega_b}\boldsymbol{E}\cdot\frac{d\boldsymbol{P_b}}{dt} \\
\frac{dN_2}{dt} &= \frac{N_3(1-N_2)}{\tau_{32}} - \frac{N_2(1-N_1)}{\tau_{21}} + \frac{1}{\hbar\omega_a}\boldsymbol{E}\cdot\frac{d\boldsymbol{P_a}}{dt} \\
\frac{dN_1}{dt} &= \frac{N_2(1-N_1)}{\tau_{21}} - \frac{N_1(1-N_0)}{\tau_{10}} - \frac{1}{\hbar\omega_a}\boldsymbol{E}\cdot\frac{d\boldsymbol{P_a}}{dt} \\
\frac{dN_0}{dt} &= \frac{N_3(1-N_0)}{\tau_{30}} + \frac{N_1(1-N_0)}{\tau_{10}} - \frac{1}{\hbar\omega_b}\boldsymbol{E}\cdot\frac{d\boldsymbol{P_b}}{dt}
\end{aligned} \tag{1}$$

where τ_{ij} is the decay time between level i and level j (i, j = 0, 1, 2, 3), ω_a is the transition frequency between level 2 and level 1, and ω_b is the transition frequency between level 3 and level 0. $\boldsymbol{E}$ represents the total electric field and can be calculated by solving the Maxwell equations. $\boldsymbol{P_a}$ and $\boldsymbol{P_b}$ correspond to the net macroscopic polarization associated with the emission and absorption transitions from level 2 to level 1 and level 3 to level 0, which are coupled with the electromagnetic fields by using the following equation [36]:

$$\begin{aligned}
\frac{d^2\boldsymbol{P_a}}{dt^2} + \gamma_{21}\frac{d\boldsymbol{P_a}}{dt} + \omega_{21}^2\boldsymbol{P_a} &= \xi_{21}(N_2 - N_1)\boldsymbol{E} \\
\frac{d^2\boldsymbol{P_b}}{dt^2} + \gamma_{30}\frac{d\boldsymbol{P_b}}{dt} + \omega_{30}^2\boldsymbol{P_b} &= \xi_{30}(N_3 - N_0)\boldsymbol{E}
\end{aligned} \tag{2}$$

where γ_{ij} is the full-widths at half-maximum for the transitions from level i to j. $\xi_{21} = 6\pi\varepsilon_0 c^3/\omega_a^2\tau_{21}$, $\xi_{30} = 6\pi\varepsilon_0 c^3/\omega_b^2\tau_{30}$. By coupling Equations (1) and (2), the amplification process of the nanolaser can be studied. The relevant parameters for R6G are as follows [38]: $\omega_a = 3.30 \times 10^{15}$ rad/s and $\omega_b = 3.68 \times 10^{15}$ rad/s, $\tau_{30} = 1$ ns, $\tau_{21} = 3$ ns, $\tau_{10} = \tau_{32} = 50$ fs, $\gamma_{21} = 1.54 \times 10^{14}$ rad/s, and $\gamma_{30} = 3.26 \times 10^{14}$ rad/s. According to the concentration of the solution prepared for the experiment, the total population density is $N = 1.89 \times 10^{24}$ m^{-3}. The x, y, and z directions of our simulation domain are set with perfectly matched layer (PML) boundary conditions. Both a total field and scatter field were set in the simulation domain.

Figure 4 presents our calculation results regarding the lasing behavior of Au NPs and MoS_2/Au NPs. Figure 4a,b depict the lasing emission spectra of Au NPs and MoS_2/Au NPs at different pump energies. It can be observed that when the pump energy is low, the emission spectrum is broad, indicating that there is no population inversion. When the pump energy reaches a certain value, the emission intensity suddenly increases, and the FWHM decreases sharply. At this point, population inversion takes place, and random lasing occurs. This pump energy is the threshold of the random laser. The normalized maximum emission intensity and the FWHM of the emission peak as a function of the pump energy are shown in Figure 4c,d. It can be distinctly seen that the threshold of the random laser based on the Au NPs and MoS_2/Au NPs are 0.734 μJ/mm^2 and 0.878 μJ/mm^2, respectively. The threshold of the random laser based on MoS_2/Au NPs is higher than that of Au NPs, which is inconsistent with the experimental result. In order to investigate the reasons for this phenomenon, we plotted the field distributions of the two structures without gain material, as shown in Figure 5a,b. The electric field localized the gap between the particles due to the coupling of the Au NP surface plasmons. The enhancement of the electric field of Au NPs relative to the background field can reach 44.5, while the field enhancement of MoS_2/Au NPs is only 37.2. This is due to the absorption loss of MoS_2. Thus, the threshold of the MoS_2/Au NPs increased in the theoretical calculations. It can be seen that if the charge transfer is not considered, the threshold will increase when Au NPs are coated with MoS_2.

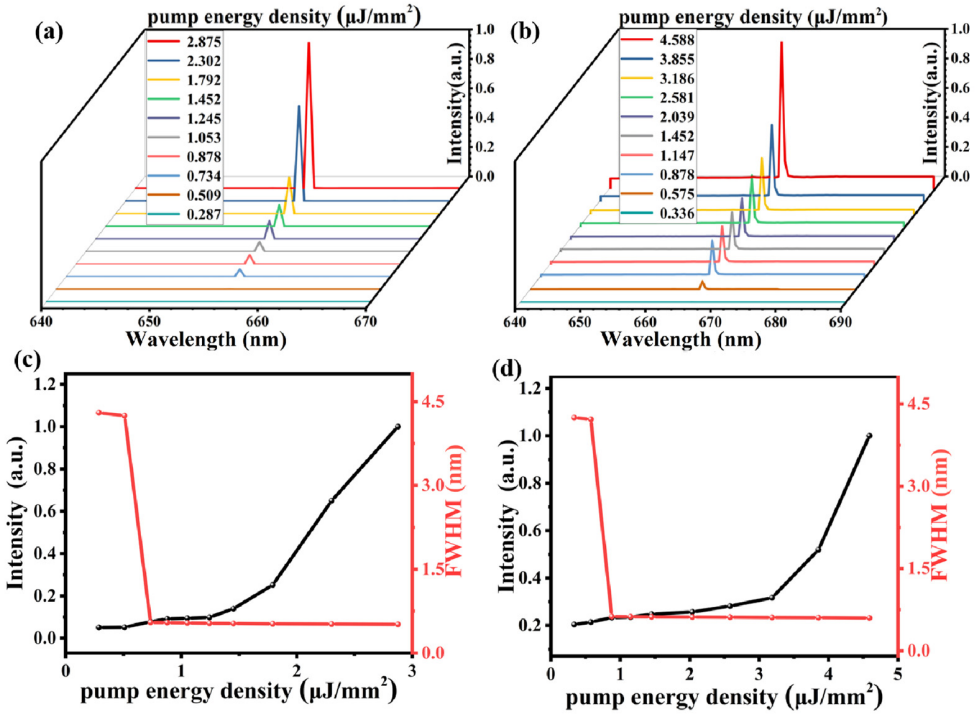

Figure 4. (**a**,**b**) The emission spectra of Au NPs (**a**) and MoS_2/Au NPs (**b**) at different pump energies. (**c**,**d**) The normalized maximum emission intensity and FWHM of the Au NPs (**c**) and MoS_2/Au NPs (**d**) emission peak as a function of pump energy.

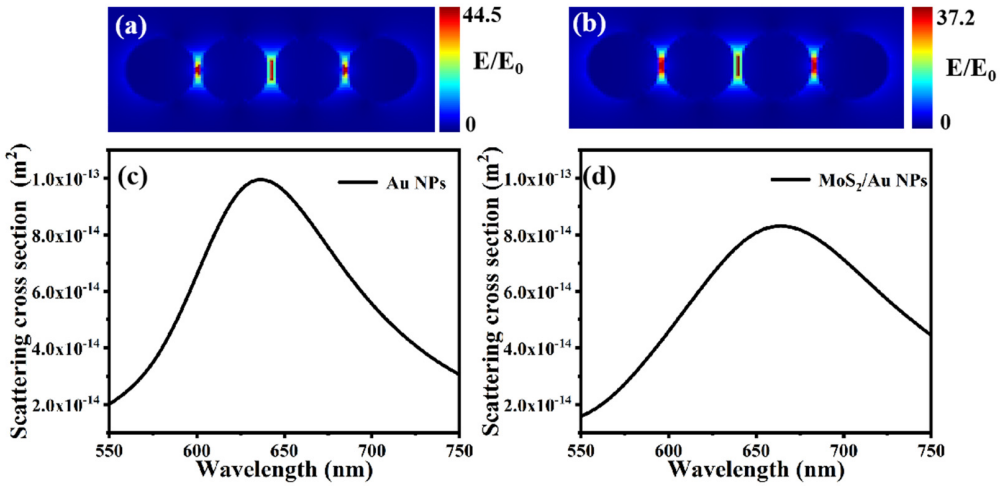

Figure 5. (**a**,**b**) Electric field distribution of Au NPs with a gap of 5 nm without (**a**) and with (**b**) MoS_2; (**c**,**d**) scattering cross-section of Au NPs without (**c**) and with MoS_2 (**d**).

The threshold of a random laser can also be affected by the scattering strength of the NPs [18]. Under the same concentration of scattered nanoparticles, the larger the scattering cross-section of the nanoparticle, the smaller the threshold of the random laser based on that nanoparticle. The scattering strength of four Au NPs and MoS_2/Au NPs was evaluated by their scattering cross-section, as shown in Figure 5c,d. We can see that when Au NPs were covered with MoS_2, the scattering cross-section was slightly reduced. Therefore, the scattering effect is not the reason for the decrease in the random laser threshold in MoS_2/Au NPs.

It has been reported that MoS_2 will transfer charge to R6G under the 532 nm excitation wavelength. And Dixit et al. reported that a charge transfer is also a random lasing

reason [31]. We investigated the effect of the charge transfer on the random laser threshold. To confirm the charge transfer mechanism between MoS_2 and R6G, we measured the PL spectra of MoS_2/Au NPs with different concentrations of R6G, as shown in Figure 6a. The PL peaks of Au NPs and MoS_2 are at 578 and 647 nm, respectively (as indicated by the fitted dotted line). Clearly, this indicates that the PL intensity of Au NPs and MoS_2 with the R6G molecule is significantly reduced at higher concentrations, indicating that both Au NPs and MoS_2 transfer charge to R6G [39]. Here, we mainly studied the effect of MoS_2 on the threshold of a random laser. The PL intensity of MoS_2 decreases with increasing R6G concentration, as the inset in Figure 6a shows, indicating that there are fewer electrons jumping from the conduction band (CB) back to the valence band (VB) for MoS_2; that is, more electrons are transferred from MoS_2 to R6G. This phenomenon is consistent with that in reference [27]. The PL spectra of R6G on both the Au NP and MoS_2/Au NP substrates are also measured in Figure 6b. It can be seen that the intensity of R6G on the MoS_2/Au NPs substrate is much stronger than that on the Au NPs substrate, which further confirms the charge transfer mechanism between MoS_2 and R6G. The band (energy level) alignment between MoS_2 and R6G is illustrated in Figure 6c. The charge transfer between the conduction band minimum (CBM) of MoS_2 and the lowest unoccupied molecular orbital (LUMO) of an R6G molecule is achieved during the excitation process with a wavelength of 532 nm [27], which results in the lower threshold of the MoS_2/Au NPs random laser.

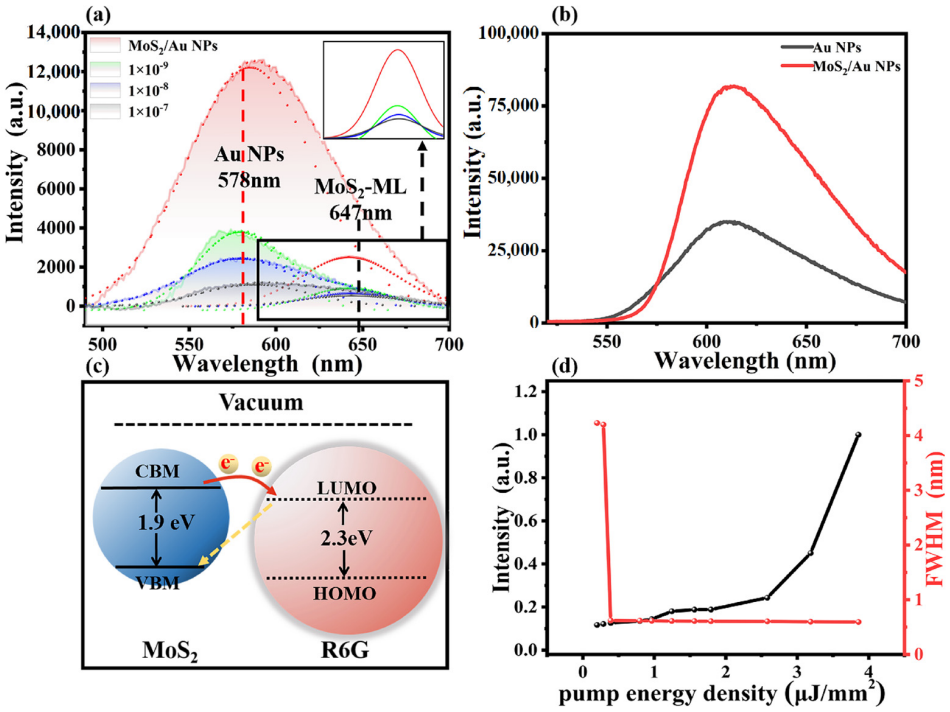

Figure 6. (**a**) PL spectra of MoS_2/Au NPs without and with R6G at different concentrations. Inset: the fitted PL spectra of MoS_2 without and with R6G at different concentrations. (**b**) PL spectra of R6G on Au NP and MoS_2/Au NP substrates. (**c**) The band alignment (energy level alignment) between R6G and MoS_2, where charge transfer is highlighted in the red path. (**d**) The normalized maximum emission intensity and FWHM of the MoS_2/Au NPs emission peak as a function of pump energy when charge transfer is considered.

An et al. performed density functional theory calculations and revealed that the CBM of MoS_2 will transfer 0.2e to the LUMO of R6G molecules under the 532 nm excitation wavelength [27], which will increase the initial population of the E_2 or E_3 level of R6G. Therefore, we added a 20% population of particles to the higher level (E_2 or E_3) of the four-level system of R6G. The calculated results are the same whether we increase the

20% population of the particles in the E_2 level or the E_3 level. The lasing action of the random laser based on MoS_2/Au NPs is calculated when the charge transfer is considered, as shown in Figure 6d. The lasing action was similar to that in Figure 4c,d, but the threshold value was reduced to 0.39 μJ/mm^2. Compared with the Au NPs without MoS_2, the lasing threshold is reduced by about 46.8%, which is essentially consistent with the experimental result. Moreover, the increase in the population in the higher energy level can also enhance the intensity of the emission peak, so the emission peak of the MoS_2/Au NPs is stronger, as shown in Figure 2c. The emission peak width of the MoS_2/Au NPs sample is broader than that of the Au NPs in the experiment, which can also be explained by charge transfer. As can be seen from the charge transfer in Figure 6c, the valence band maximum (VBM) of MoS_2 is close to the highest occupied molecular orbital (HOMO) of R6G. When the electrons transfer from LUMO to HOMO of R6G, they can also transfer to the VBM of MoS_2 (as the yellow dotted line shown), which leads to an increase in the emission spectral width. It can be seen from the above that charge transfer is the reason for the lower threshold of the MoS_2/Au NPs random laser.

It is worth noting that the threshold of the random laser we calculated theoretically is lower than the experimental results because we set the gap between the Au NPs to 5 nm during the above-mentioned theoretical calculation, which results in a strong electric field enhancement between the Au NPs. As shown in Figure 7a, when the gap is increased to 10 nm, the enhancement of the electric field of Au NPs decreases to 19.2, and the threshold of the random laser increases to 1.369 μJ/mm^2. The random laser action of Au NPs coated with MoS_2 is shown in Figure 7b, and its threshold is 0.719 μJ/mm^2, which also reduces by 47.4%. We also calculated the lasing behavior of a single Au NP, as shown in Figure 7c,d. The enhancement of the electric field decreases to 4.4, and the threshold of the random laser increases to 1.561 μJ/mm^2. When Au NPs are coated with MoS_2, the threshold is reduced to 0.828 μJ/mm^2, which also reduces by 46.9%, which is still consistent with the experimental results. The enhancement of the electric field affects only the threshold of the nanolaser but does not affect the effect of charge transfer on the threshold.

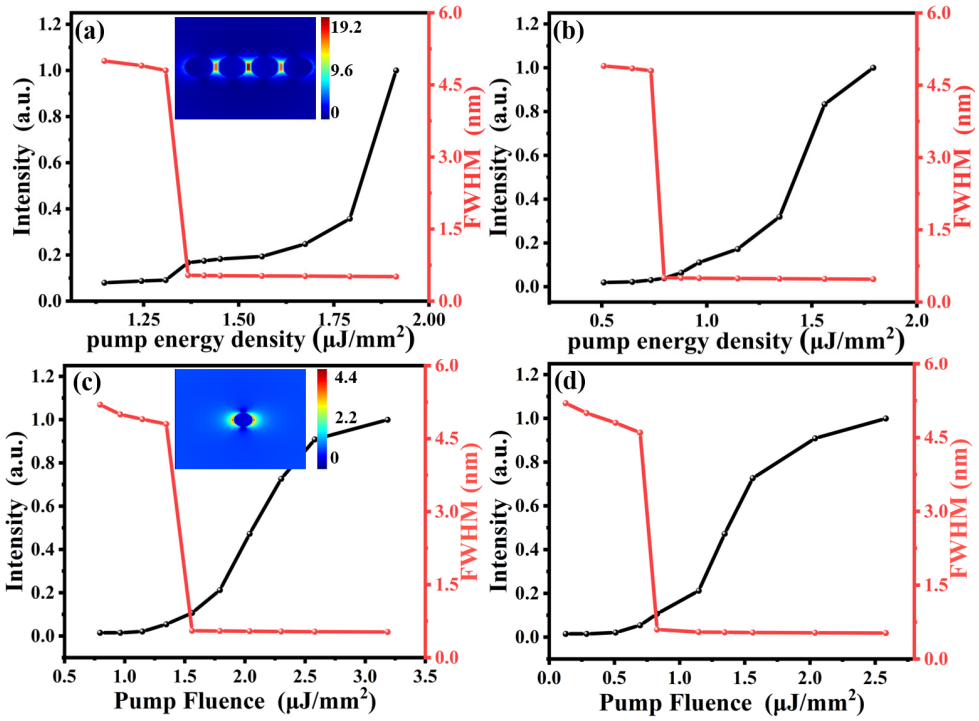

Figure 7. The normalized maximum emission intensity and FWHM of the emission peak as a function of pump energy for four Au NPs (**a**,**b**) and a single Au NP (**c**,**d**) without (**a**,**c**) and with MoS_2 (**b**,**d**). Inset: The electric field distribution of Au NPs with a gap of 10 nm and a single Au NP.

4. Conclusions

In summary, we successfully synthesized the MoS_2/Au NPs composite structure through annealing $(NH_4)_2MoS_4$ on Au NPs and studied the lasing action of a random laser based on them. By comparing the lasing measurements of Au NPs and MoS_2/Au NPs, we studied the effect of MoS_2 on the threshold of the random laser. The results showed that the addition of MoS_2 reduced the random laser threshold. Compared to the Au NPs sample, the threshold was reduced by 46.2%. Through theoretical calculation, it was found that the electric field and scattering cross-section decreased after MoS_2 was added, which did not lead to a decrease in the random laser threshold. The combined experimental and computational study demonstrates that charge transfer is the dominant mechanism behind the reduction in threshold for the MoS2/Au NPs random laser. A 20% population of particles was added to the E_2 or E_3 energy level of the four-level two-electron model of R6G. The calculated threshold can be reduced by about 46.8% compared to Au NPs samples, which is consistent with the experimental results. This study provides a convenient and efficient method for the study of random lasers based on novel 2D materials and metallic nanostructures and provides a technological route to realize low-threshold, high-performance random lasers.

Author Contributions: Y.H., Z.L. and Y.R. proposed the project. K.S. conducted the equation derivation and simulation and wrote the manuscript. Y.W., L.Z. and T.N. helped to modify the manuscript. Y.Z., W.L. and J.W. helped to translate the paper and conduct a relevant literature search. All authors have read and agreed to the published version of the manuscript.

Funding: The National Natural Science Foundation of China (12274271, 12174228, 12104268) and the Natural Science Foundation of Shandong Province (ZR2023MA073, ZR2021ZD02).

Institutional Review Board Statement: Not applicable.

Informed Consent Statement: Not applicable.

Data Availability Statement: The data supporting the findings of this study are available within the article.

Conflicts of Interest: The authors declare no conflicts of interest.

References

1. Bian, Y.; Xue, H.; Wang, Z. Programmable Random Lasing Pluses Based on Waveguide-Assisted Random Scattering Feedback. *Laser Photonics Rev.* **2021**, *15*, 2000506. [CrossRef]
2. Consoli, A.; Caselli, N.; López, C. Electrically driven random lasing from a modified Fabry–Pérot laser diode. *Nat. Photonics* **2022**, *16*, 219–225. [CrossRef]
3. Luan, F.; Gu, B.; Gomes, A.S.; Yong, K.T.; Wen, S.; Prasad, P.N. Lasing in nanocomposite random media. *Nano Today* **2015**, *10*, 168–192. [CrossRef]
4. Azmi, A.N.; Wan Ismail, W.Z.; Abu Hassan, H.; Halim, M.M.; Zainal, N.; Muskens, O.L.; Wan Ahmad Kamil, W.M. Review of open cavity random lasers as laser-based sensors. *ACS Sens.* **2022**, *7*, 914–928. [CrossRef] [PubMed]
5. Gomes, A.S.; Moura, A.L.; de Araújo, C.B.; Raposo, E.P. Recent advances and applications of random lasers and random fiber lasers. *Prog. Quantum Electron.* **2021**, *78*, 100343. [CrossRef]
6. Gummaluri, V.S.; Nair, R.V.; Krishnan, S.R.; Vijayan, C. Femtosecond laser-pumped plasmonically enhanced near-infrared random laser based on engineered scatterers. *Opt. Lett.* **2017**, *42*, 5002–5005. [CrossRef]
7. Haddawi, S.F.; Humud, H.R.; Hamidi, S.M. Tunable low power piezo-plasmonic random laser under external voltage. *Optik* **2020**, *207*, 164482. [CrossRef]
8. Xia, J.Y.; He, J.J.; Xie, K.; Zhang, X.J.; Hu, L.; Li, Y.X.; Chen, X.; Ma, J.; Wen, J.; Chen, J.; et al. Replica symmetry breaking in FRET-assisted random laser based on electrospun polymer fiber. *Ann. Phys.* **2019**, *531*, 1900066. [CrossRef]
9. Li, Y.; Xie, K.; Zhang, X.; Hu, Z.; Ma, J.; Chen, X.; Zhang, J.; Liu, Z.; Chen, D. Coherent Random Lasing Realized in Polymer Vesicles. *Photonic Sens.* **2019**, *10*, 254–264. [CrossRef]
10. Goldberg, I.; Annavarapu, N.; Leitner, S.; Elkhouly, K.; Han, F.; Verellen, N.; Kuna, T.; Qiu, W.; Rolin, C.; Genoe, J.; et al. Multimode Lasing in All-Solution-Processed UV-Nanoimprinted Distributed Feedback MAPbI3 Perovskite Waveguides. *ACS Photonics* **2023**, *10*, 1591–1600. [CrossRef]
11. Shi, X.; Chang, Q.; Bian, Y.; Cui, H.; Wang, Z. Line Width-Tunable Random Laser Based on Manipulating Plasmonic Scattering. *ACS Photonics* **2019**, *6*, 2245–2251. [CrossRef]
12. Ejbarah, R.A.; Jassim, J.M.; Hamidi, S.M. The effect of dye concentration and cell thickness on dye–polymer random laser action. *Opt. Quantum Electron.* **2021**, *53*, 116. [CrossRef]

13. Gayathri, R.; Monika, K.; Murukeshan, V.M.; Vijayan, C. Low threshold incoherent random lasing with spectral overlap optimization of size-tuned plasmonic nanorods. *Opt. Laser Technol.* **2021**, *139*, 106959. [CrossRef]
14. Zhao, Q.; Ye, L.; Cheng, Z.; Hong, S.; Penty, R.; White, I. Random lasing action from PMMA waveguide doped with CdSe/ZnS CQDs plasmonically enhanced by Ag nanoislands. *Opt. Laser Technol.* **2020**, *131*, 106358. [CrossRef]
15. Wan, Y.; Wang, H.; Li, H.; Ye, R.; Zhang, X.; Lyu, J.; Cai, Y. Low-threshold random lasers enhanced by titanium nitride nanoparticles suspended randomly in gain solutions. *Opt. Express* **2022**, *30*, 8222–8233. [CrossRef] [PubMed]
16. Zhang, N.; Ning, S.; Dai, K.; Zhang, Y.; Wu, Y.; Yuan, F.; Zhang, F. Random lasing based on a nanoplasmonic hybrid structure composed of (Au core)-(Ag shell) nanorods with Ag film. *Opt. Mater. Express* **2020**, *10*, 1204–1214. [CrossRef]
17. Xu, L.; Li, F.; Wei, L.; Zhou, J.; Liu, S. Design of Surface Plasmon Nanolaser Based on MoS_2. *Appl. Sci.* **2018**, *8*, 2110. [CrossRef]
18. Wan, Y.; Li, X.; Wang, Y.; Li, Z.; Liu, X.; Cai, Y. Low-threshold random lasers based on the DCM-DEG gain system with graphene nanosheets. *Opt. Express* **2023**, *31*, 6713–6721. [CrossRef] [PubMed]
19. Shen, Y.L.; Shi, B.R.; Lv, H.; Zhang, S.Y.; Wang, X. Graphene-based Au nanoparticle enhanced dye random laser. *Acta Phys. Sin.* **2022**, *71*, 034206. [CrossRef]
20. Roy, P.K.; Haider, G.; Lin, H.I.; Liao, Y.M.; Lu, C.H.; Chen, K.H.; Chen, L.C.; Shih, W.H.; Liang, C.T.; Chen, Y.F. Multicolor Ultralow-Threshold Random Laser Assisted by Vertical-Graphene Network. *Adv. Opt. Mater.* **2018**, *6*, 1800382. [CrossRef]
21. Yang, F.; Cheng, S.; Zhang, X.; Ren, X.; Li, R.; Dong, H.; Hu, W. 2D organic materials for optoelectronic applications. *Adv. Mater.* **2018**, *30*, 1702415. [CrossRef]
22. Shangguan, Q.; Zhao, Y.; Song, Z.; Wang, J.; Yang, H.; Chen, J.; Yi, Z. High sensitivity active adjustable graphene absorber for refractive index sensing applications. *Diam. Relat. Mater.* **2022**, *128*, 109273. [CrossRef]
23. Xu, X.; Liu, L. MoS_2 with Controlled Thickness for Electrocatalytic Hydrogen Evolution. *Nanoscale Res. Lett.* **2021**, *16*, 137. [CrossRef]
24. Zhou, Y.; Liu, Y.; Zhang, M.; Han, Q.; Wang, Y.; Sun, X.; Zhang, X.; Dong, C.; Sun, J.; Tang, Z.; et al. Rationally designed hierarchical N, P co-doped carbon connected 1T/2H-MoS_2 heterostructures with cooperative effect as ultrafast and durable anode materials for efficient sodium storage. *Chem. Eng. J.* **2022**, *433*, 133778. [CrossRef]
25. Nalwa, H.S. A review of molybdenum disulfide (MoS_2) based photodetectors: From ultra-broadband, self-powered to flexible devices. *RSC Adv.* **2020**, *10*, 30529–30602. [CrossRef]
26. Chen, Y.; Sun, M. Two-dimensional WS_2/MoS_2 heterostructures: Properties and applications. *Nanoscale* **2021**, *13*, 5594–5619. [CrossRef]
27. An, K.; Chen, M.; He, B.; Ai, H.; Wang, W.; Zhang, Z.; Pan, Z.; Chen, S.; Ip, W.F.; Lo, K.H.; et al. Wafer-Scale 2H-MoS_2 Monolayer for High Surface-enhanced Raman Scattering Performance: Charge-Transfer Coupled with Molecule Resonance. *Adv. Mater. Technol.* **2022**, *7*, 2200217. [CrossRef]
28. Sun, L.; Hu, H.; Zhan, D.; Yan, J.; Liu, L.; Teguh, J.S.; Yeow, E.K.L.; Lee, P.S.; Shen, Z. Plasma Modified MoS_2 Nanoflakes for Surface Enhanced Raman Scattering. *Small* **2014**, *10*, 1090–1095. [CrossRef]
29. Li, Z.; Jiang, S.; Xu, S.; Zhang, C.; Qiu, H.; Li, C.; Sheng, Y.; Huo, Y.; Yang, C.; Man, B. Few-layer MoS_2-encapsulated Cu nanoparticle hybrids fabricated by two-step annealing process for surface enhanced Raman scattering. *Sens. Actuators B Chem.* **2016**, *230*, 645–652. [CrossRef]
30. Jayasekara, C.; Premaratne, M.; Gunapala, S.D.; Stockman, M.I. MoS_2 spaser. *J. Appl. Phys.* **2016**, *13*, 133101. [CrossRef]
31. Dixit, T.; Arora, A.; Krishnan, A.; Ganapathi, K.L.; Nayak, P.K.; Rao, M.S.R. Near Infrared Random Lasing in Multilayer MoS_2. *ACS Omega* **2018**, *3*, 14097–14102. [CrossRef]
32. Zhai, T.; Zhang, X.; Pang, Z.; Su, X.; Liu, H.; Feng, S.; Wang, L. Random Laser Based on Waveguided Plasmonic Gain Channels. *Nano Lett.* **2011**, *11*, 4295–4298. [CrossRef]
33. Cui, Y.; Wang, J.; Li, Y.; Wu, Y.; Been, E.; Zhang, Z.; Cui, Y. Twisted epitaxy of gold nanodisks grown between twisted substrate layers of molybdenum disulfide. *Science* **2024**, *383*, 212–219. [CrossRef]
34. Bornacelli, J.; Torres-Torres, C.; Silva-Pereyra, H.; Labrada-Delgado, G.; Crespo-Sosa, A.; Cheang-Wong, J.; Oliver, A. Superlinear photoluminescence by ultrafast laser pulses in dielectric matrices with metal nanoclusters. *Sci. Rep.* **2019**, *9*, 5699. [CrossRef]
35. Ziegler, J.; Djiango, M.; Vidal, C.; Hrelescu, C.; Klar, T.A. Gold nanostars for random lasing enhancement. *Opt. Express* **2015**, *23*, 15152–15159. [CrossRef]
36. Chang, S.H.; Taflove, A. Finite-difference time-domain model of lasing action in a four-level two-electron atomic system. *Opt. Express* **2004**, *16*, 3827–3833. [CrossRef]
37. Yan, M.; Sun, K.; Ning, T.; Zhao, L.; Ren, Y.; Huo, Y. Numerical study of low threshold nanolasers based on quasi continuous beam binding of resonant waveguide grating structures. *Acta Phys. Sin.* **2023**, *4*, 044202. [CrossRef]
38. Hakala, T.K.; Rekola, H.T.; Väkeväinen, A.I.; Martikainen, J.P.; Nečada, M.; Moilanen, A.J.; Törmä, P. Lasing in dark and bright modes of a finite-sized plasmonic lattice. *Nat. Commun.* **2017**, *8*, 13687. [CrossRef]
39. Sun, H.; Yao, M.; Song, Y.; Zhu, L.; Dong, J.; Liu, R.; Li, P.; Zhao, B.; Liu, B. Pressure-induced SERS enhancement in a MoS_2/Au/R6G system by a two-step charge transfer process. *Nanoscale* **2019**, *11*, 21493–21501. [CrossRef]

Disclaimer/Publisher's Note: The statements, opinions and data contained in all publications are solely those of the individual author(s) and contributor(s) and not of MDPI and/or the editor(s). MDPI and/or the editor(s) disclaim responsibility for any injury to people or property resulting from any ideas, methods, instructions or products referred to in the content.